SIAM J. APPL. MATH.
Vol. 67, No. 4, pp. 1166–1182

COMPUTATION OF EXTENSIONAL FALL OF SLENDER VISCOUS DROPS BY A ONE-DIMENSIONAL EULERIAN METHOD*

B. H. BRADSHAW-HAJEK†, Y. M. STOKES†, AND E. O. TUCK†

Abstract. We develop a one-dimensional Eulerian model suitable for analyzing the behavior of viscous fluid drops falling from rest from an upper boundary. The method allows examination of development and behavior from early time, when a drop and filament begin to form, out to large times when the bulk of the fluid forms a drop at the bottom of a long thin filament which connects it with the upper boundary. This model overcomes problems seen in Lagrangian models, caused by excessive stretching of grid elements, and enables a better examination of the thin fluid filament.

Key words. extensional flow, dripping, moving boundary, viscous flow, free surface

AMS subject classifications. 35K55, 35Q30, 35R35, 76M20, 76D08

DOI. 10.1137/050646743

1. Introduction. Formation of drops via extensional flow and break-off has been much studied (see the review article by Eggers [6]), motivated by a wide range of applications such as ink-jet printing, spinning and drawing of polymer or glass fibers, glass blowing and blow-molding in the manufacture of containers, light bulbs and glass tubing, rheological measurement by fiber extension, and fiber spinning for polymers and glasses [3, 4, 9, 13]. Considerable progress has been made towards an understanding of the breakup of a thin filament into drops, although the exact details of the final stages of breakup are yet to be resolved. However, the evolution of the drop and filament from some initial configuration, and the influence of initial conditions on the final breakup, are still relatively unexplored and have been the focus of our attention for some time [15, 14]. Some work by others on this topic includes [20, 18].

The problem of interest is a drop of very viscous fluid hanging beneath a solid wall/boundary and extending under gravity, similar to honey dripping from an upturned spoon. Analyses with and without inertia have been done and compared by the present authors [15, 14]. Surface tension was neglected in those studies, on the basis that a mean diameter $\ell = \sqrt{R_0 L_0}$ of the drop is large compared to the meniscus scale $\sqrt{\gamma/(\rho g)}$, or equivalently that the Bond number $Bo = \rho g \ell^2/\gamma$ is large. Here g is the gravitational acceleration, ρ, γ are respectively the density and surface tension coefficient of the fluid, R_0 is a length scale for the drop's cross section (e.g., the radius of the drop at the wall), and L_0 is the initial length of the drop. As the fluid filament extends and gets thinner, this neglect of surface tension may become less justifiable, and an examination of the effect of surface tension is desirable.

Because of the slender geometries involved, one-dimensional models are common in analysis of filament breakup [8, 1, 19, 5, 7, 17, 11]. However, the development of a drop and filament may also involve nonslender geometries at early times, requiring numerical solution of the full Navier–Stokes equations. Our previous work [15, 14] has involved both one-dimensional models and numerical solution of the Navier–Stokes

*Received by the editors December 5, 2005; accepted for publication (in revised form) February 5, 2007; published electronically May 29, 2007. This work was supported by Australian Research Council Discovery grant DP0450047.

http://www.siam.org/journals/siap/67-4/64674.html

†Department of Applied Mathematics, University of Adelaide, SA 5005, Australia (bronwyn.hajek@adelaide.edu.au, Yvonne.Stokes@adelaide.edu.au, ernie.tuck@adelaide.edu.au).

equations for axisymmetric drops and two-dimensional sheets.

For all of our work, a Lagrangian reference frame has been used, with grids that move with moving fluid elements. However, as the filament thins and surface tension potentially becomes important, Lagrangian numerics begin to fail due to the stretching of the grid. For example, in finite-element simulations of the full Navier–Stokes equations [14], mesh elements in and near the filament region become excessively elongated or distorted, leading to loss of accuracy. Similarly, in one-dimensional models the grid points become sparse in the filament region while congregating in the main drop, so that we lose the ability to examine the development of the filament. Hence, if we are to better investigate the filament evolution, including possible effects of surface tension, we must modify our methods.

A number of techniques are available to address the resolution problem in the filament region. First, we can begin with an irregular mesh that has a concentration of grid points in the section of the drop that will develop into the filament region. This, however, will only be successful until that section of the mesh becomes very stretched. Another option is to remesh when grid points become too sparse in the filament. This method becomes difficult (although not impossible) with the inclusion of inertia (see, for example, [18]), as all unknowns and their time derivatives must be interpolated from the old mesh onto the new mesh. In this paper, we wish to present a further alternative in which the congregation of mesh points does not occur.

We have therefore developed a one-dimensional model in an Eulerian reference frame, where the Lagrangian coordinate (a fluid particle label equal to the initial distance ξ from the wall) is sought as a function of time t and that particle's physical distance x from the wall. This model may be derived directly from the Navier–Stokes and continuity equations, as described below. It may also be obtained (in the absence of surface tension) by a transformation of our previous one-dimensional Lagrangian model [14] for the cross-sectional area A as a function of time t and Lagrangian coordinate ξ, which will also be outlined here.

The resulting PDE for $\xi = Z(x,t)$ is formally of higher order in space than the original PDE for $A(\xi,t)$. Also, while the original problem could be solved in a fixed spatial domain $0 < \xi < L_0$, where L_0 is the initial drop length, the transformation results in a moving boundary problem in the domain $0 < x < L(t)$, where the actual drop length $L(t)$ must be determined as part of the problem. Both of these aspects mean that the problem in physical coordinates is considerably harder to solve than that in Lagrangian coordinates, but it has the major benefit that grid elements do not become stretched over time and is therefore worth pursuing in order to better understand the filament behavior.

The increased complexity of the problem is partly a result of the transformation employed, with a further element of difficulty added by the inclusion of surface tension. In the absence of surface tension, the equations may be directly integrated, simplifying the numerical problem. In this paper we explore the new model and its solution in the absence of surface tension, which will be considered in a future paper. We will, however, derive here the equations with surface tension included.

2. A one-dimensional Eulerian model. For an axisymmetric column of incompressible fluid, a one-dimensional lubrication approximation to the Navier–Stokes equations yields (see, for example, [5, 11, 10])

$$\frac{\partial u}{\partial t} + u\frac{\partial u}{\partial x} = g - \frac{\gamma}{\rho}\frac{\partial K}{\partial x} + \frac{\nu^*}{h^2}\frac{\partial}{\partial x}\left(h^2\frac{\partial u}{\partial x}\right), \tag{2.1}$$

while the continuity equation becomes

$$(h^2)_t + (uh^2)_x = 0, \tag{2.2}$$

where subscripts denote derivatives, $\nu_* = 3\mu/\rho$ is the elongational (Trouton) kinematic viscosity [16] of a fluid with shear viscosity μ and density ρ, g is gravitational acceleration in the downward (positive) direction, γ is the coefficient of surface tension, $u(x,t)$ is the downward velocity of the fluid at position x and time t, $h(x,t)$ is the radius of the drop, and $K(x,t)$ is the curvature of the drop, given by

$$K = \frac{1}{\sqrt{1+(h_x)^2}}\left[\frac{1}{h} - \frac{h_{xx}}{1+(h_x)^2}\right]. \tag{2.3}$$

The cross-sectional area of the drop is given by $A = \pi h^2$, so (2.2) can be rewritten as

$$A_t + uA_x = -Au_x \tag{2.4}$$

and substituted into (2.1) to obtain

$$u_t + uu_x = g - \frac{\gamma}{\rho}K_x - \frac{\nu^*}{A}\frac{\partial}{\partial x}\left(\frac{\partial A}{\partial t} + u\frac{\partial A}{\partial x}\right)$$

or

$$\frac{Du}{Dt} = g - \frac{\gamma}{\rho}K_x - \frac{\nu^*}{A}\frac{\partial}{\partial x}\frac{DA}{Dt}, \tag{2.5}$$

where $D/Dt = \partial/\partial t + u\,\partial/\partial x$ denotes the material time derivative.

In a Lagrangian reference frame [15, 14, 19] we let $x = X(\xi,t)$, where ξ is a fluid-particle label such that $x = \xi$ at $t = 0$. The initial drop geometry is assumed to have a cross-sectional area distribution given by some function $A_0(\xi)$. That is, $A(\xi,0) = A_0(\xi)$, $0 \le \xi \le L_0$, where $A(\xi,t)$ is the cross-sectional area at label ξ and time t, and L_0 is the initial drop length. Conservation of mass demands [14]

$$A\frac{\partial X}{\partial \xi} = A_0$$

or, on integration,

$$X(\xi,t) = \int_0^\xi \frac{A_0(\xi_1)}{A(\xi_1,t)}d\xi_1. \tag{2.6}$$

Now, defining $\xi = Z(x,t)$, we have

$$A = A_0 Z_x, \quad u = X_t = -\frac{Z_t}{Z_x}, \quad \text{and} \quad \frac{\partial A_0}{\partial x} = A_0' Z_x,$$

where primes denote differentiation with respect to ξ. Substituting for A and u in (2.5) gives

$$\begin{aligned} -\frac{D}{Dt}\left(\frac{Z_t}{Z_x}\right) &= g - \frac{\gamma}{\rho}K_x - \frac{\nu^*}{A_0 Z_x}\frac{\partial}{\partial x}\left[A_0\frac{D}{Dt}(Z_x)\right] \\ &= g - \frac{\gamma}{\rho}K_x - \nu^*\left[\frac{A_0'}{A_0}\frac{D}{Dt}(Z_x) + \frac{1}{Z_x}\frac{\partial}{\partial x}\left(\frac{D}{Dt}(Z_x)\right)\right] \\ &= g - \frac{\gamma}{\rho}K_x - \nu^*\frac{D}{Dt}\left(\frac{A_0'}{A_0}Z_x + \frac{Z_{xx}}{Z_x}\right), \end{aligned} \tag{2.7}$$

with

$$\frac{D}{Dt} = \frac{\partial}{\partial t} - \frac{Z_t}{Z_x}\frac{\partial}{\partial x}.$$

The transformation to the dependent variable $Z(x,t)$ has yielded a PDE (2.7) that is second order in time and third order in space, whereas the Navier–Stokes equation (2.1) is first order in time and second order in space. The main reason for this increase in order is that the dependant variable is a position rather than a velocity (as in the Navier–Stokes equations). In order to solve (2.7), we must also solve for the length of the drop $L(t) = X(L_0, t)$, which is increasing with time. Thus, we need two initial conditions and four boundary conditions. One initial condition is obtained from the definition of the Lagrangian coordinate such that $\xi = x$ at $t = 0$, so that

$$Z(x,0) = x. \tag{2.8}$$

The other comes from the condition that the flow starts from rest, so $u(x,0) = 0$ or

$$Z_t(x,0) = 0. \tag{2.9}$$

With respect to boundary conditions, two (one at each end) come from the definition of the Lagrangian coordinate such that $x = 0$ at $\xi = 0$ and $x = L(t)$ at $\xi = L_0$, giving

$$Z(0,t) = 0, \tag{2.10}$$

$$Z(L(t),t) = L_0. \tag{2.11}$$

Since the drop is falling from under a solid plane boundary where the normal velocity is zero for all time, i.e., $u = 0$ at $x = 0$, then $Du/Dt = 0$ at $x = 0$, and hence, from (2.7),

$$0 = g - \frac{\gamma}{\rho}K_x - \nu^* \frac{D}{Dt}\left(\frac{A_0'}{A_0}Z_x + \frac{Z_{xx}}{Z_x}\right) \quad \text{at} \quad x = 0. \tag{2.12}$$

We require a further boundary condition which comes from a balance between viscous stresses and surface tension at the bottom of the drop $x = L(t)$. One-dimensional theory yields

$$\frac{\partial}{\partial x}\left(\frac{Z_t}{Z_x}\right) = -\frac{\gamma}{\rho\nu^*}K, \quad \text{or, equivalently,} \quad \frac{D}{Dt}(Z_x) = -\frac{\gamma}{\rho\nu^*}Z_x K. \tag{2.13}$$

Equation (2.7) subject to initial and boundary conditions (2.8)–(2.13) describes the fall of a drop of viscous fluid from underneath a solid boundary, starting from a known initial configuration. Gravitational, viscous, inertial, and surface tension effects are all included. The model derived involves the fluid-particle label $\xi = Z(x,t)$ as the dependent variable, with the physical space coordinate x and time t as the independent variables.

For zero surface tension ($\gamma = 0$), (2.7) simplifies considerably, by integration with respect to the material time derivative. With nonzero surface tension ($\gamma \neq 0$), such a procedure is computationally problematic due to the necessity of time-integrating the surface-tension term while holding the particle label $\xi = Z(x,t)$ constant. We leave consideration of this matter to a future paper and, from here on, neglect surface

tension (i.e., set $\gamma = 0$). Integration with respect to t at fixed $\xi = Z$, subject to $Z = x$ and $Z_t = 0$ at $t = 0$, then yields

$$-\frac{Z_t}{Z_x} = gt - \nu^* \left(\frac{A_0'}{A_0}(Z_x - 1) + \frac{Z_{xx}}{Z_x} \right)$$

or

$$Z_t = \nu^* Z_{xx} - gtZ_x - \nu^* \frac{A_0'(Z)}{A_0(Z)} Z_x(1 - Z_x). \tag{2.14}$$

Equation (2.14) is in general a nonlinear PDE which, like the Navier–Stokes equation (2.1), is first order in time and second order in space. It is worth noting in passing that in the special case of an initially cylindrical drop where $A_0 =$ constant, it becomes linear, and in the further special case where gravity can be neglected (such as in a liquid bridge problem [2]), it reduces to the ordinary linear heat-conduction equation, with diffusivity ν^*.

The appropriate initial and boundary conditions are

$$\begin{aligned} Z(x,0) &= x \qquad \text{at } t = 0, \\ Z(0,t) &= 0 \qquad \text{at } x = 0, \\ Z(L(t),t) &= L_0 \qquad \text{at } x = L(t), \\ Z_x(L(t),t) &= 1 \qquad \text{at } x = L(t). \end{aligned} \tag{2.15}$$

Note that we no longer need boundary condition (2.12), which in integrated form is equivalent to $u = 0$ at $x = 0$, and which is automatically satisfied by demanding $Z(0,t) = 0$. Also, with $\gamma = 0$, (2.13) can be integrated with respect to the material time derivative to give $Z_x = 1$ at $x = L(t)$ as we have in (2.15).

The Lagrangian equivalent to (2.14) in terms of the cross-sectional area $A(\xi, t)$ as a function of Lagrangian coordinate ξ and time t is readily (by manipulation of (2.14)) shown to be

$$u = gt - \frac{\nu^*}{A_0} \frac{\partial}{\partial \xi}(A - A_0).$$

Differentiating with respect to ξ, using (2.6), and rearranging gives

$$\frac{\partial A}{\partial t} = \nu_* \frac{A^2}{A_0} \frac{\partial}{\partial \xi} \left(\frac{1}{A_0} \frac{\partial}{\partial \xi}(A - A_0) \right), \quad 0 \le \xi \le L_0. \tag{2.16}$$

The corresponding initial and boundary conditions are

$$A(\xi,0) = A_0(\xi), \quad \frac{\partial}{\partial \xi}(A - A_0)(0,t) = \frac{gt}{\nu^*} A_0(0), \quad A(L_0,t) = A_0(L_0). \tag{2.17}$$

The Lagrangian model given by (2.16) and (2.17) was derived directly in [14] by balancing viscous and gravitational forces; the inertialess version was considered in [15]. Comparison between solutions to these models and those for the new Eulerian model of present interest, (2.14) and (2.15), will be given below. We note that the Eulerian model involves gravity explicitly in the PDE (2.14), whereas the Lagrangian model involves gravity only in a boundary condition at $\xi = 0$ (2.17).

3. Eulerian-model solution. For the remainder of this paper, we will be primarily interested in initially paraboloidal slender drops, given in Lagrangian coordinates by $A_0(\xi) = A_0(0)(1 - \xi/L_0)$ with small aspect ratio $\alpha_r = \sqrt{A_0(0)}/L_0 \ll 1$, as considered in [14].

Defining dimensionless variables (denoted by bars)

$$\overline{A}_0(\overline{\xi}) = \frac{A_0(\xi)}{A_0(0)}, \quad \overline{\xi} = \overline{Z} = \frac{\xi}{L_0} = \frac{Z}{L_0}, \quad \overline{x} = \frac{x}{L_0}, \quad \overline{t} = \frac{gL_0}{\nu^*}t, \tag{3.1}$$

the dimensionless form of (2.14) for the initially paraboloidal drop $\overline{A}_0(\overline{Z}) = 1 - \overline{Z}$ is (after removing the bars)

$$Re\, Z_t = Z_{xx} - tZ_x + \frac{Z_x}{1 - Z}[1 - Z_x], \tag{3.2}$$

with the Reynolds number Re given by

$$Re = \frac{gL_0^3}{\nu^{*2}}.$$

The initial and boundary conditions (2.15) become

$$Z(x,0) = x, \quad Z(0,t) = 0, \quad Z(L(t),t) = 1, \quad \text{and} \quad Z_x(L(t),t) = 1. \tag{3.3}$$

Equation (3.2) subject to (3.3) is most easily solved using the explicit forward-time-centered-space finite difference method. Setting the time step Δt and spatial step Δx, we approximate (3.2) in the usual manner by

$$\begin{aligned} Re\frac{Z_i^{j+1} - Z_i^j}{\Delta t} &= \frac{Z_{i+1}^j - 2Z_i^j + Z_{i-1}^j}{\Delta x^2} - t\frac{Z_{i+1}^j - Z_{i-1}^j}{2\Delta x} \\ &\quad + \frac{1}{1 - Z_i^j}\frac{Z_{i+1}^j - Z_{i-1}^j}{2\Delta x}\left[1 - \frac{Z_{i+1}^j - Z_{i-1}^j}{2\Delta x}\right], \end{aligned} \tag{3.4}$$

where $Z_i^j = Z(x_i, t_j)$ is the value of $Z(x,t)$ at the jth time step and the ith grid point. For numerical stability, we must ensure that the diffusion number $\Delta t/Re(\Delta x)^2 < 0.5$.

The initial and wall boundary conditions are easily specified by setting $Z_i^0 = i\Delta x$ and $Z_0^j = 0$. However, the boundary conditions at the free end are not quite so straightforward to implement, due to the moving boundary. At each time step, the drop becomes longer and some of the drop (at the bottom) will move beyond the current computational domain. Hence we need to extend the grid to the new position of the bottom of the drop.

Specifically, having computed Z_i^{j+1}, $i = 1, \ldots, N_j - 1$, using (3.4), we seek an extrapolation procedure that approximates the bottom of the drop, satisfying the boundary conditions $Z = Z_x = 1$ at the (as yet unknown) drop bottom $x = L(t_{j+1})$, and that matches our already computed solution above the bottom. The most obvious choice is a linear polynomial extrapolation, but this can only be first order accurate, and we prefer to preserve the second order accuracy of the finite difference scheme. To achieve this, we could seek a quadratic polynomial extrapolation

$$Z(x, t_{j+1}) = a_{j+1}(x - x_{N_j - 1})^2 + b_{j+1}(x - x_{N_j - 1}) + c_{j+1},$$

where the unknown coefficients $a_{j+1}, b_{j+1}, c_{j+1}$ and the unknown length $L(t_{j+1})$ of the drop are determined by satisfying the two boundary conditions at $x = L(t)$ and

matching the already computed solution at x_{N_j-2} and x_{N_j-1}. An equally good second order extrapolation is to use the exponential approximation

$$Z(x,t_{j+1}) = e^{x-L(t_{j+1})}, \quad \text{where} \quad e^{-L(t_{j+1})} = Z_{N_j-1}^{j+1} e^{-x_{N_j-1}}. \tag{3.5}$$

In fact, (3.5) is just the local form of the solution from the corresponding Lagrangian model neglecting inertia as in [15], and hence has a stronger physical motivation than the quadratic extrapolant.

Earlier work [15, 14] has shown that, with neglect of surface tension, the drop shape very near to the bottom is given quite accurately by the inertialess solution. This is because at early times, accelerations are very small and Stokes flow solutions are applicable; at later times, the main drop is essentially in free fall and (with neglect of surface tension) does not change in shape. Furthermore, for some initial configurations, including the initially paraboloidal drop considered here, we can obtain an exact analytic solution to the Lagrangian model neglecting inertia and use this to assign appropriate values of $Z(x,t)$ to the new grid points. Specifically, using (3.1), the dimensionless form of the Lagrangian PDE (2.16) is (after removing the bars)

$$Re\frac{\partial A}{\partial t} = \frac{A^2}{A_0}\frac{\partial}{\partial \xi}\left(\frac{1}{A_0}\frac{\partial}{\partial \xi}(A - A_0)\right), \quad 0 \le \xi \le 1, \tag{3.6}$$

with initial and boundary conditions

$$A(\xi,0) = A_0(\xi), \quad \frac{\partial}{\partial \xi}(A - A_0)(0,t) = t, \quad A(1,t) = A_0(1,t). \tag{3.7}$$

In the inertialess limit ($Re = 0$) this has the explicit solution

$$A(\xi,t) = A_0(\xi) - tV(\xi), \quad V(\xi) = \int_\xi^1 A_0(\xi_1)\, \mathrm{d}\xi_1. \tag{3.8}$$

As discussed by Stokes, Tuck, and Schwartz [15], the cross-sectional area of the drop vanishes at the position $\xi = \xi_*$ such that $t = t_* = A_0(\xi_*)/V(\xi_*)$ is a minimum, so that the drop formally breaks with $A(\xi_*, t_*) = 0$. The time t_* is the "crisis" time; at this time the length of the drop, given by (2.6) with $\xi = 1$, formally becomes infinite in this inertialess approximation. No solution exists for $t > t_*$; i.e., we have a finite-time blow up at the crisis time t_*. However, for larger times $t > t_*$ the main drop is effectively falling as a solid body, and in the absence of surface tension it retains the same shape given by (3.8) with $t = t_*$.

For the initially paraboloidal drop $A_0(\xi) = 1 - \xi$, (3.8) becomes

$$A(\xi,t) = (1-\xi)\left(1 - \frac{1}{2}t(1-\xi)\right), \tag{3.9}$$

from which we see that $\xi_* = 0$ and $t_* = 2$; i.e., the drop breaks at the wall at the crisis time $t = 2$. Hence, for all $t \ge 2$,

$$A(\xi) = \xi(1-\xi), \tag{3.10}$$

which is a solution to (3.6). It is readily verified using $Z_x = A/A_0$ that (3.9) satisfies the condition $Z_x = 1$ at $x = L(t)$ (i.e., $\xi = 1$) for all $t \le 2$.

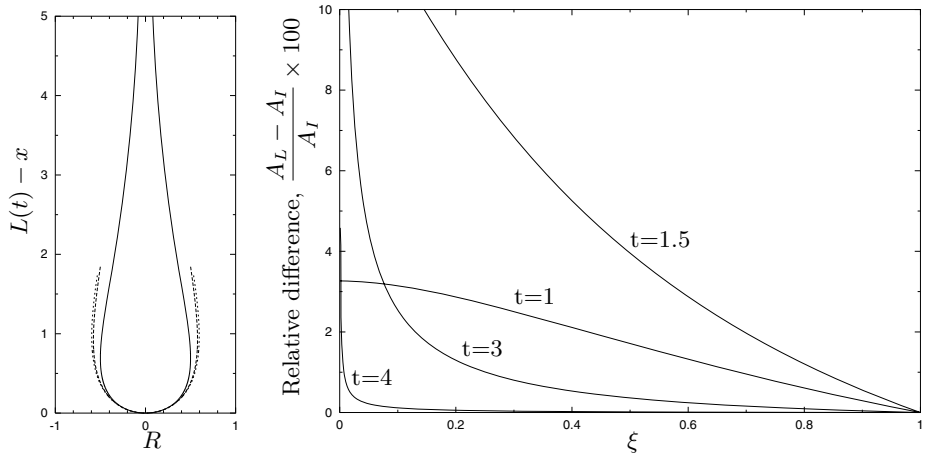

FIG. 3.1. (a) *Drop shape as a function of distance* $L(t) - x$ *from the bottom of the drop. Inertialess solution* (3.9) *at* $t = 1.5$ *(solid); solution to the Lagrangian PDE* (3.6) *at* $t = 1.5$ *(dotted) and* $t = 4.0$ *(dashed); the inertialess large-time solution* (3.10) *is indistinguishable from the dashed curve.* (b) *Percentage relative difference between the solution to the Lagrangian PDE* (3.6) *and the inertialess solution* (3.9) *for* $t < 2$ *or* (3.10) *for* $t \geq 2$. *The percentage relative difference is calculated as* $100 \times (A_L - A_I)/A_I$, *where* A_L *is the calculated solution to* (3.6) *and* A_I *is the inertialess solution* (3.9) *or* (3.10). *Here* (3.6) *was solved using implicit backward differencing with* $Re = 0.1$, $\Delta\xi = 10^{-3}$, $\Delta t = 10^{-3}$.

The extrapolant for $Z(x,t)$ is obtained by substituting $A_0 = 1 - Z$, and $A(Z,t)$ given by (3.9) for $t < 2$ or (3.10) for $t \geq 2$, into $Z_x = A/A_0$. Integrating then yields

$$Z(x,t) = \begin{cases} 1 - \dfrac{2}{t} + c(t)\,\mathrm{e}^{xt/2} & \text{for } \ 0 < t < 2, \\ c(t)\,\mathrm{e}^{x} & \text{for } \ t \geq 2. \end{cases} \tag{3.11}$$

We solve for the value of the unknown function of time $c(t)$ at time t_{j+1} using the already computed value of Z at x_{N_j-1}. The expression so obtained for $t \geq 2$ is (3.5) exactly. It is also readily seen that the expression obtained for $t < 2$ is second-order accurate. Thus, we use (3.11) to calculate values of $Z^{j+1}_{N_j+k}$, $k = 0, 1, \ldots$, stopping when $Z^{j+1}_{N_j+k} > 1$, and thus extending the computational domain to N_{j+1} grid points. The actual position of the bottom of the drop is given by solving $Z(L(t_{j+1}), t_{j+1}) = 1$.

The accuracy of this procedure is demonstrated for $Re = 0.1$ in Figure 3.1. Figure 3.1(a) compares the drop shape at $t = 1.5$ given by the inertialess solution (3.9) and as found by solving (3.6); also shown is the large- (i.e., crisis) time inertialess solution (3.10), which is indistinguishable from the solution to (3.6) at $Re = 0.1$, $t = 4$. Figure 3.1(b) shows the percentage relative difference between solutions to (3.6) at Reynolds number $Re = 0.1$ and the inertialess solution at different times. At the very bottom of the drop, the relative difference is much less than 1%. As the Reynolds number increases, the inertialess solution becomes less accurate as a global approximation for the drop shape, but each (dimensionless) time step represents a decreasing physical time interval so that still only very few grid points are extrapolated. Even for Reynolds numbers as high as $Re = 10$, it gives a good approximation for the local region near the bottom of the drop. Thus the method remains (second-order) accurate. In fact, because only a very few grid points are ever extrapolated, the choice of extrapolation procedure has only a minor effect on the solution.

Having determined the Lagrangian coordinate $Z(x,t)$ over the new, extended, computational domain, the actual shape of the drop can be calculated via $R = \sqrt{A} = \sqrt{A_0 Z_x}$.

4. Results and comparison between Eulerian and Lagrangian models. The numerical solution to (3.2) for the particle label $Z(x,t)$ as a function of physical space and time is shown, for Reynolds number $Re = 0.1$, in Figure 4.1. The growth of the computational domain as a result of the moving boundary at $Z = 1$ can be clearly seen.

The axisymmetric drop shape is shown in Figure 4.2(a), alongside drop shapes from the numerical solution to the Lagrangian equation (3.6), in Figure 4.2(b). The solution to (3.6) was calculated using the implicit backward-time-centered-space finite difference method. The two different models produce the same drop shapes with the same overall length; however, there are some differences to be highlighted.

First, for times $t \gtrsim 2.6$ the computed solutions to the Lagrangian model (Figure 4.2(b)) appear to move away from the wall. This is due to stretching of the grid and a consequent loss of grid points in the filament region and accumulation of grid points in the main drop below the filament, as seen in Figure 4.3(b). The fluid particle that is initially a distance $x = \Delta\xi$ from the wall (i.e., the closest point to the wall for which we calculate $A(\xi,t)$) falls ever downwards, so that there is a continually lengthening region in physical space, which is essentially the fluid filament connecting the drop to the wall, about which we know virtually nothing. Unfortunately, it is in this filament region that our greatest interest lies, since this is where the drop will eventually break. While decreasing the grid spacing near the wall will extend the time over which we have near complete information, there will always come a time (soon after the crisis time t_* of the inertialess theory, when accelerations approach gravitational acceleration) when the grid becomes too stretched in the filament region. This loss of information in the filament region is completely overcome with the Eulerian model (Figure 4.2) because gridpoints are fixed in space and the grid constantly extended as the drop length increases. This leads to a uniform spacing of grid points over the full

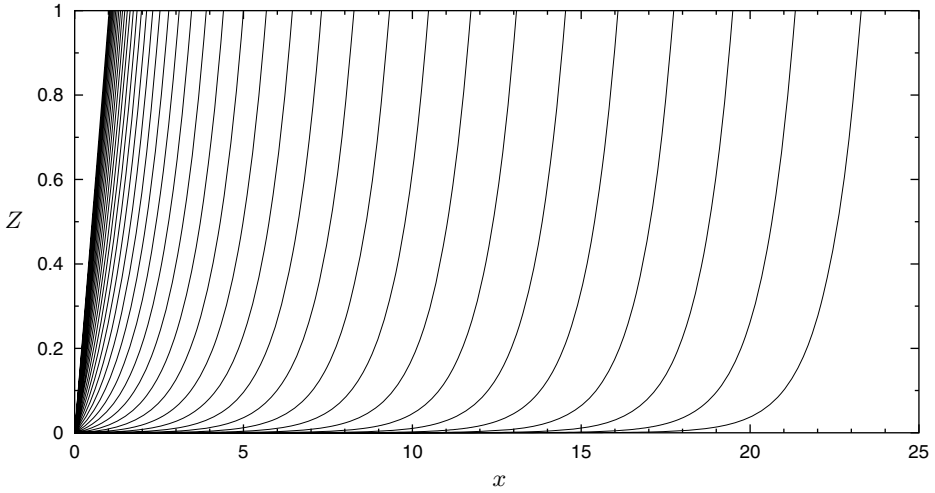

FIG. 4.1. *Solution to PDE* (3.2) *for* $Z(x,t)$*, with* $Re = 0.1$*, at times* $t = 0, 0.1, \ldots, 3.9, 4.0$*. Here* $\Delta x = 10^{-2}$*,* $\Delta t = 4 \times 10^{-6}$*.*

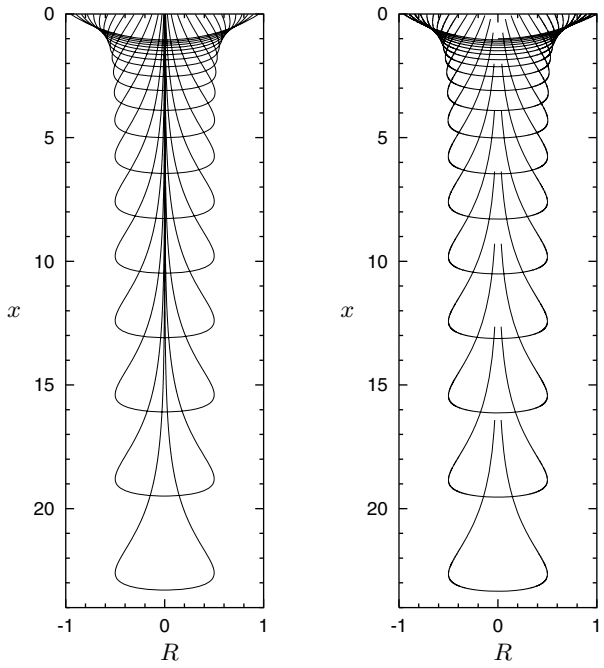

FIG. 4.2. *Drop shapes for* $Re = 0.1$ *at times* $t = 0, 0.2, \ldots, 3.8, 4.0$. (a) *Shape calculated using Eulerian framework* (3.2) *(*$\Delta x = 10^{-2}$, $\Delta t = 4. \times 10^{-6}$*).* (b) *Shape calculated using Lagrangian framework* (3.6) *(*$\Delta\xi = 10^{-3}$, $\Delta t = 10^{-3}$*).*

length of the drop, as seen in Figure 4.3(a). The greater knowledge of the filament region that results from the Eulerian model will better enable a future study of the effect of surface tension on filament breakup and drop pinch-off.

A second point of difference between the Eulerian and Lagrangian models is with respect to the behavior near the wall boundary at $x = \xi = 0$. At this boundary, the Lagrangian boundary condition (3.7) for the initially paraboloidal drop is

$$\frac{\partial A}{\partial \xi}(0,t) + 1 = t. \tag{4.1}$$

For the Lagrangian model it is a simple matter to check that this boundary condition is indeed satisfied, by computing $A_\xi(0,t)$ using the forward-space finite difference formula, i.e.,

$$A_\xi(0,t) = \frac{A(\Delta\xi, t) - A(0,t)}{\Delta\xi}.$$

The value of $A_\xi(0,t) + 1$ so computed is plotted against time t in Figure 4.4 (solid curve). The wall boundary condition is satisfied until $t \approx 2.0$ and then $A_\xi(i,t)$ begins to move away from t. At $t \approx 2.4$ there is a rapid deviation from the correct solution as the value of $A_\xi(0,t)$ decreases and appears to approach a constant unit value. This highlights the fact that the Lagrangian solution cannot be relied upon at large times when the grid becomes excessively stretched in physical space.

The equivalent condition on $A_\xi(0,t)$ for the Eulerian model is obtained by differ-

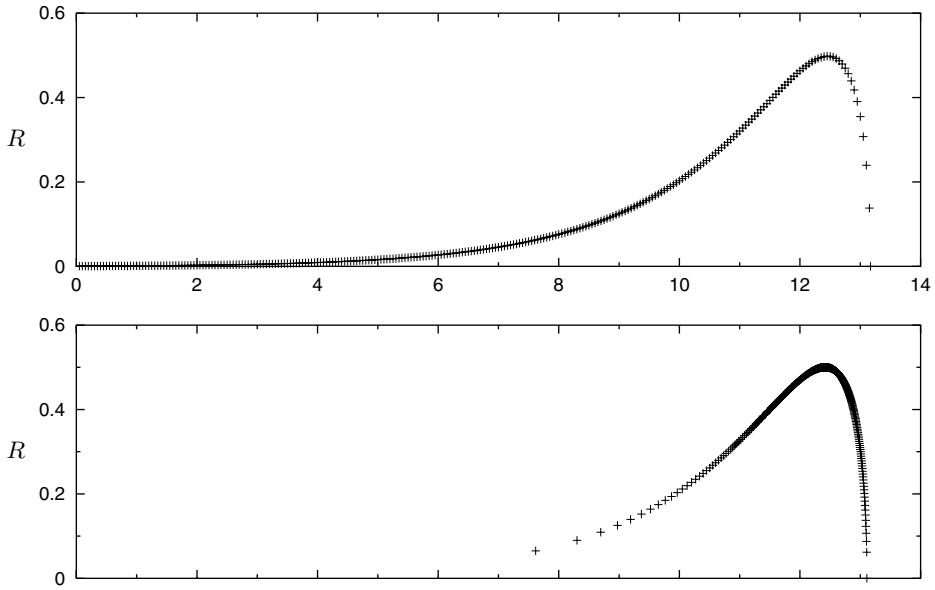

FIG. 4.3. *Comparison of Lagrangian and Eulerian solution methods at* $t = 3.4$. *Each figure has approximately* 260 *grid points.* (a) *Drop shape calculated using the Eulerian model* (3.2), (3.3) *(*$\Delta x = 5 \times 10^{-2}$, $\Delta t = 10^{-4}$*).* (b) *Drop shape calculated using the Lagrangian model* (3.6), (3.7) *(*$\Delta x = 1/260$, $\Delta t = 10^{-3}$*). The extra grid points in the filament region of the Eulerian model can be clearly seen.*

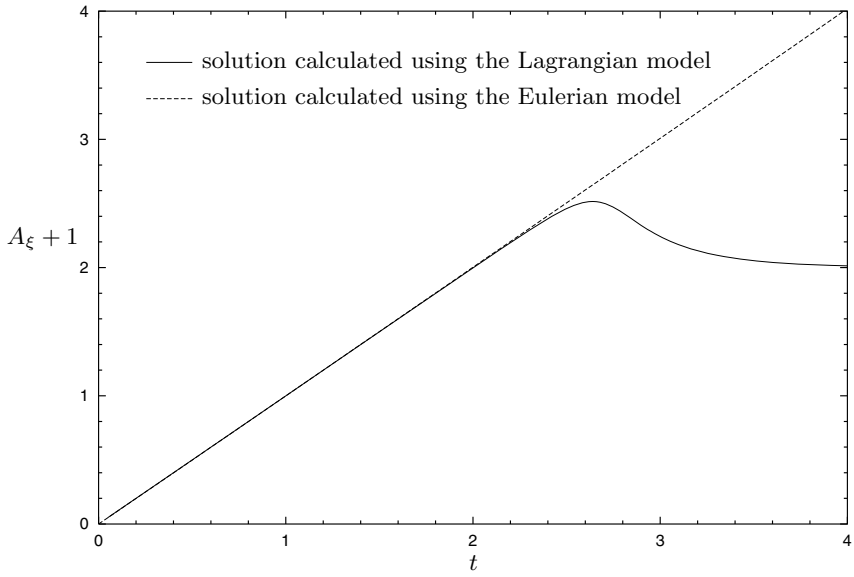

FIG. 4.4. *The accuracy of the Lagrangian and Eulerian models as indicated by the wall boundary condition* $(3.7)_2$. *For an initially paraboloidal drop we require* $A_\xi + 1 \sim t$. *This condition is satisfied by the Eulerian model but not the Lagrangian model.*

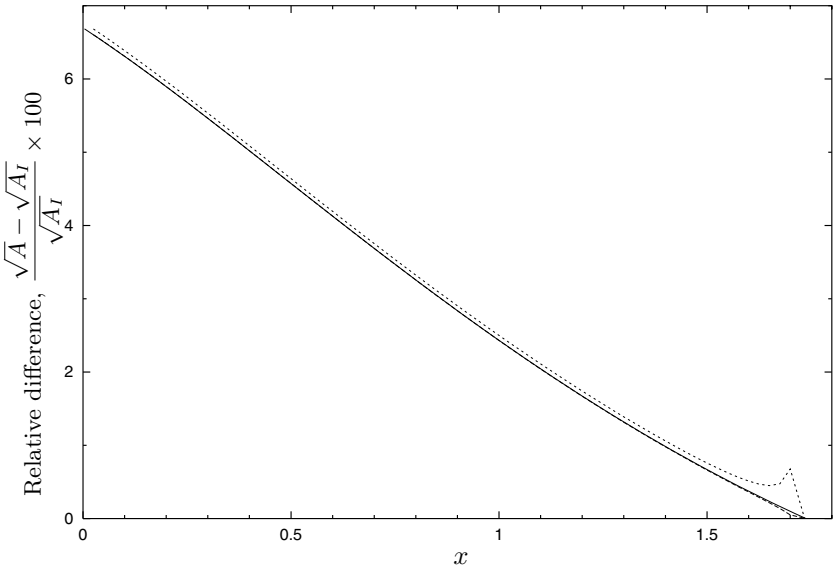

FIG. 4.5. *Percentage relative differences at $t = 1.5$ between the inertialess radius $\sqrt{A_I}$ with A_I given by (3.9), and Lagrangian and Eulerian solutions with $Re = 0.1$. The difference is given by $100 \times (\sqrt{A} - \sqrt{A_I})/\sqrt{A_I}$, where A denotes the Lagrangian solution (solid), the Eulerian solution with extension of the computational domain using the inertialess solution at crisis time (dashed), and the Eulerian solution with extension of the computational domain using the forward-difference representation of $Z_x(L(t), t) = 1$ (dotted).*

entiating $A = A_0 Z_x$ with respect to ξ, i.e. (for the initially paraboloidal drop),

$$\begin{aligned} A_\xi &= A_0' Z_x + \frac{A_0 Z_{xx}}{Z_x} \\ &= -Z_x + (1 - Z)\frac{Z_{xx}}{Z_x}. \end{aligned}$$

The slope, A_ξ at the wall can thus be found from the calculated values of $Z(0, t)$, $Z(\Delta x, t)$, and $Z(2\Delta x, t)$ using first order forward-space finite difference formulae for Z_x and Z_{xx}, i.e.,

$$Z_x(0, t) = \frac{Z(\Delta x, t) - Z(0, t)}{\Delta x} \quad \text{and} \quad Z_{xx}(0, t) = \frac{Z(2\Delta x, t) - 2Z(\Delta x, t) + Z(0, t)}{\Delta x^2}.$$

Figure 4.4 (dashed line) shows that $A_\xi + 1 \sim t$ for times well beyond $t = 2.4$; i.e., the wall boundary condition (4.1) is satisfied. Thus, we see that, for large times, the solution obtained from the Eulerian model is more reliable than that obtained from the Lagrangian model, especially in the filament region.

This is also shown by Figures 4.5 and 4.6. Figure 4.5 shows the relative differences between the inertialess prediction (3.9) of the drop/filament radius ($R = \sqrt{A}$) and solutions at $Re = 0.1$ to the Lagrangian and Eulerian models, as a function of physical distance x from the upper wall boundary, at time $t = 1.5$ before the crisis time of inertialess theory. There is excellent agreement between the Lagrangian and Eulerian models at this time, with a difference visible only at the very bottom of the drop. Figure 4.6 gives the same comparisons but at time $t = 4$, well after the crisis time of inertialess theory. Now we see considerably more difference between the Lagrangian

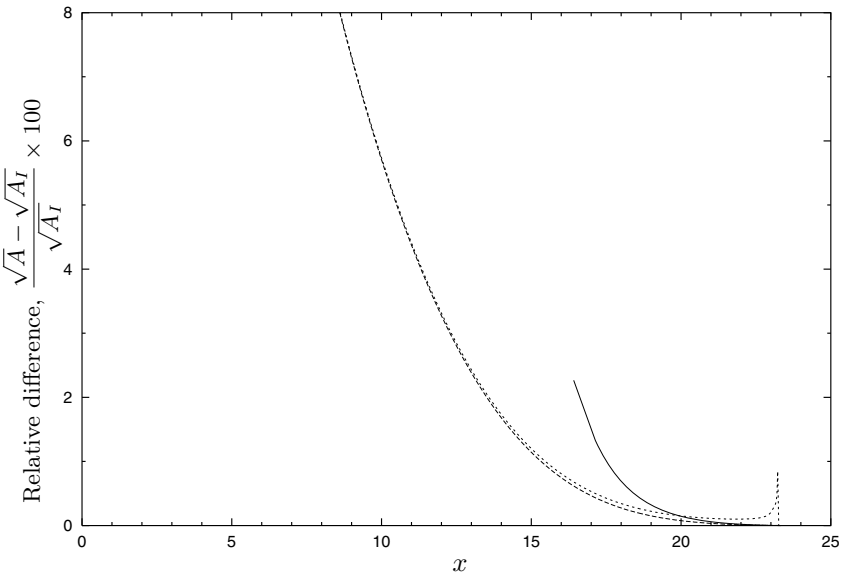

FIG. 4.6. *As for Figure* 4.5 *but at time* $t = 4$*, with* A_I *given by the inertialess large-time solution* (3.10).

and Eulerian solutions, which is due to error in the Lagrangian solution resulting from an excessively stretched grid. Note also that grid stretching limits our comparison to the bottom third of the drop where the Lagrangian solution is available; in the region $0 \leq x < 16$ no information is available from the Lagrangian solution due to a lack of grid points.

For interest, Figures 4.5 and 4.6 also show results for the Eulerian solution obtained using the finite difference approximation to the boundary condition $Z_x = 1$ at $x = L(t)$, discussed earlier as an alternative to pasting of the inertialess solution to the bottom of the drop. This differs from the other curves by only about 0.1% over most of the drop length, with the difference increasing to about 1% at the very bottom; note that the overall drop length is slightly less, as mentioned earlier, although it is not noticable with the grid size used here or at the scales shown.

It is interesting to note that at small Reynolds number the time at which the numerical solution to (3.6) begins to become inaccurate in the filament region (as indicated by Figure 4.4) is approximately equal to the crisis time of inertialess theory, as predicted in [15] ($t_* = 2$), when accelerations increase rapidly up to gravitational acceleration. This correlation between the inertialess crisis time and the time at which the small-Reynolds-number Lagrangian solution becomes inaccurate is also observed with other initial drop shapes.

5. Discussion and conclusions. The major benefit of reformulating the extensional flow problem using an Eulerian framework is that, in contrast to other one-dimensional Lagrangian models, we now include many grid points in the filament region. The Eulerian scheme is computationally more costly, as there is a rapid increase in the number of grid points as the computational domain extends with the falling drop. However, this method provides us with information about the filament region which we cannot obtain using a Lagrangian method. Accuracies such as those achieved in Figure 4.2 can still be obtained in a matter of minutes. This greater res-

olution in the filament region enables us to better study the dynamics and behavior of the developing filament. In particular we are now much better equipped to investigate the effects of surface tension on the filament, the drop shape, and pinch-off of the main drop by solving (2.7) with $\gamma \neq 0$. This will be considered in a future paper.

Meanwhile, reformulating the problem also enables us to address a question previously posed in Stokes and Tuck [14]. In that paper, we saw that at small Reynolds numbers and large times, the main part of the drop is indistinguishable from a solid object that fell from rest at an apparent time t_0. Identification of this apparent time with the crisis time of inertialess theory leads to the conclusion that the large-time drop shape is the drop shape obtained at the crisis time when neglecting inertia. Conversely, it can be shown that equating the large-time drop shape at small Reynolds numbers with the drop shape at the crisis time of inertialess theory, which is strongly supported by the numerical solutions (both here and in [14]), implies that the apparent time t_0 and the crisis time t_* are identical. This relationship between the inertialess theory and the large-time limit of the flow with inertia implies the expected large-time shape for an initially paraboloidal drop [14]

$$A(x,t) = \mathrm{e}^{-(L-x)}\left[1 - \mathrm{e}^{-(L-x)}\right], \tag{5.1}$$

where $L = L(t)$ is the length of the drop at time t. However, the asymptotic theory described in [14] did not provide an estimate of the actual length $L(t)$ of the drop. We can now supply that estimate.

In the physical coordinate system, the cross-sectional area of the drop is given by $A(x,t) = A_0 Z_x$. The expected large-time drop shape obtained from the inertialess theory, for the initially paraboloidal drop, is given by $(3.11)_2$ as $Z(x,t) = c(t)\mathrm{e}^x$, so that

$$\begin{aligned} A(x,t) &= (1 - Z)Z_x \\ &= (1 - c(t)\,\mathrm{e}^x)c(t)\,\mathrm{e}^x. \end{aligned} \tag{5.2}$$

Comparing this with (5.1), we see that

$$c(t) = \mathrm{e}^{-L(t)} \quad \text{or} \quad L(t) = -\ln c(t). \tag{5.3}$$

Furthermore, since $(3.11)_2$ must be a solution to the PDE in physical coordinates, we may substitute it into (3.2) to obtain a first order differential equation for $c(t)$. Upon solving this, we find

$$c(t) = \exp\left[-\frac{1}{2Re}(t-2)^2 - \widetilde{L}_0\right], \tag{5.4}$$

where $\widetilde{L}_0$ is a constant. The length of the drop at large times is then given by

$$L(t) = \frac{1}{2Re}(t-2)^2 + \widetilde{L}_0, \tag{5.5}$$

and the velocity of the bottom of the drop can be found by differentiating to get

$$L'(t) = \frac{1}{Re}(t-2). \tag{5.6}$$

The constant $\widetilde{L}_0$ is seen to be the apparent initial length of the drop at the crisis time $t_* = 2$ of inertialess theory when the main drop essentially enters free fall from rest. That is, at later times, the bottom of the drop falls as if it were dropped from rest at time t_* with apparent initial length $\widetilde{L}_0$.

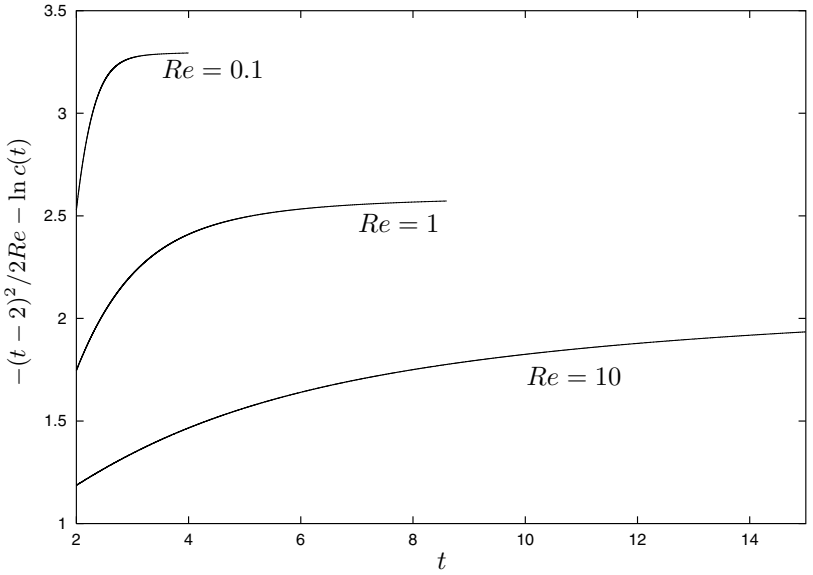

FIG. 5.1. *Plot of the function* $-(t-2)^2/(2Re) - \ln c(t)$ *for* $Re = 0.1, 1.0, 10$, *which at large time* t *gives the apparent initial length* $\widetilde{L}_0$ *of an initially paraboloidal drop. We obtain* $\widetilde{L}_0 \approx 3.3$ *for* $Re = 0.1$, $\widetilde{L}_0 \approx 2.6$ *for* $Re = 1.0$, *and* $\widetilde{L}_0 \approx 2.0$ *for* $Re = 10$.

Our solution of the Eulerian model for initially paraboloidal slender drops involves computation of the function $c(t)$ for extension of the computational domain. Then, at large time, an approximate value for the apparent initial length is given by

$$\widetilde{L}_0 = -\frac{1}{2Re}(t-2)^2 - \ln c(t).$$

With Reynolds numbers $Re = 0.1, 1.0, 10$, we find $\widetilde{L}_0 \approx 3.3, 2.6, 2.0$ (see Figure 5.1). As the Reynolds number increases we must compute to (dimensionless) times well beyond the crisis time $t_* = 2$ of inertialess theory to determine $\widetilde{L}_0$. Figure 5.2 shows $Re\left(L(t) - \widetilde{L}_0\right)$, $Re = 0.1, 1, 10$, versus time t, where $L(t)$ is the length of the drop found by solving (3.2) as described above. At large time this approaches $(t-2)^2/2$, as predicted by (5.5), although, again, as the Reynolds number increases we must compute to times increasingly larger than the crisis time of the inertialess limit to see the agreement.

Another point of interest is that the large-time drop (5.1) (Lagrangian coordinates) or (5.2) (Eulerian coordinates), which derives from the inertialess large-time drop shape (3.10) is observed to be a good representation for the main body of the drop and the lower portion of the filament, as seen by a comparison of Figures 4.6 and 4.2(a); the inertialess large- (crisis) time solution is accurate to within 1% over $x > 15$ (see Figure 4.6), which we see from Figure 4.2(a) is over the bottom third of the drop and filament at this time. The inertialess solution is less accurate in the upper filament region, which is to be expected since inertia and viscous fluid flow are significant in this region of transition from rigid body motion (at increasing velocity) back to zero velocity at the wall; the inertialess solution can be justified only at early time when accelerations are much smaller than gravity, or at larger times in the main drop region which is falling as a rigid body.

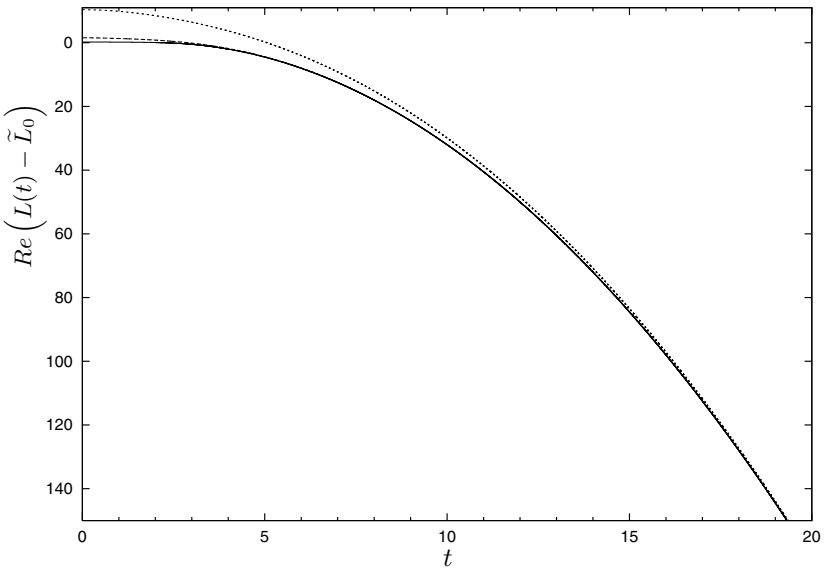

FIG. 5.2. *Plot of* $Re(L(t) - \widetilde{L}_0)$ *with* $L(t)$ *found by solving* (3.2) *for* $Re = 0.1$ *(solid),* 1.0 *(dashed), and* 10 *(dotted), and as predicted at large times* $t > 2$ *by* (5.5), $(t-2)^2/2$ *(solid).*

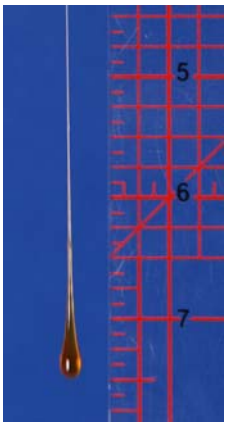

FIG. 5.3. *Dripping golden syrup from a knife. The drop shape is paraboloidal, in contrast to the globular shape of glycerine dripping from a capillary tube as in* [12]. *Note that the scale is in inches.*

Finally we consider the extent to which our computed drop shapes agree with observation. Typically, photographs of viscous fluid drops in the literature (e.g., as in [12]) are of liquids like glycerine dripping from a capillary tube. These drops appear to be considerably more globular in shape than those computed here, but this is essentially a matter of initial conditions. For glycerine-like drops, the initial drop shape is determined by (essentially static) capillarity, as the drop forms slowly at the bottom of the capillary, so that it begins its fall with an already quite globular shape. On the other hand, in the present paper we are assuming an initial shape which is paraboloidal, which is quite like that seen for larger and more viscous drops of liquids like honey falling from a knife or upturned spoon (Figure 5.3). The initial

shape of such rapidly formed drops is influenced very little by surface tension, and their subsequent shape in fall is then quite like those presented here.

Acknowledgments. We gratefully acknowledge valuable discussions with Prof. P. Broadbridge and Dr. Michael Teubner. We are also grateful to an anonymous referee whose helpful comments have resulted in an improved paper.

REFERENCES

[1] L. E. Cram, *A numerical model of droplet formation*, in Computational Techniques & Applications: CTAC-83, J. Noye and C. Fletcher, eds., Elsevier Science/North–Holland, Amsterdam, 1984, pp. 182–188.
[2] P. Concus, R. Finn, and J. McCuan, *Liquid bridges, edge blobs, and Scherk-type capillary surfaces*, Indiana Univ. Math. J., 50 (2001), pp. 411–441.
[3] J. DeWynne, J. R. Ockendon, and P.Wilmott, *On a mathematical model for fiber tapering*, SIAM J. Appl. Math., 49 (1989), pp. 983–990.
[4] P. J. Doyle, *Glass Making Today*, Portcullis Press, Surrey, UK, 1994.
[5] J. Eggers, *Universal pinching of* $3D$ *axisymmetric free surface flow*, Phys. Rev. Lett., 71 (1993), pp. 3458–3460.
[6] J. Eggers, *Nonlinear dynamics and breakup of free surface flows*, Rev. Modern Phys., 69 (1997), pp. 865–929.
[7] J. Eggers and T. F. Dupont, *Drop formation in a one-dimensional approximation of the Navier-Stokes equation*, J. Fluid Mech., 262 (1994), pp. 205–221.
[8] M. A. Matovich and J. R. A. Pearson, *Spinning a molten threadline*, Indust. Engrg. Chem. Fundamentals, 8 (1969), pp. 512–520.
[9] J. E. Matta and R. P. Titus, *Liquid stretching using a falling cylinder*, J. Non-Newton. Fluid, 35 (1990), pp. 215–229.
[10] W. W. Schultz and S. H. Davis, *One-dimensional liquid fibers*, J. Rheol., 26 (1982), pp. 331–345.
[11] S. Senchenko and T. Bohr, *Shape and stability of a viscous thread*, Phys. Rev. E (3), 71 (2005), paper 56301.
[12] X. Shi, M. P. Brenner, and S. R. Nagel, *A cascade of structure in a drop falling from a faucet*, Science, 265 (1994), pp. 219–222.
[13] T. Sridhar, V. Tirtaatmadja, D. A. Nguyen, and R. K. Gupta, *Measurement of extensional viscosity of polymer solutions*, J. Non-Newton. Fluid, 40 (1991), pp. 271–280.
[14] Y. M. Stokes and E. O. Tuck, *The role of inertia in extensional fall of a viscous drop*, J. Fluid Mech., 498 (2004), pp. 205–225.
[15] Y. M. Stokes, E. O. Tuck, and L. W. Schwartz, *Extensional fall of a very viscous fluid drop*, Quart. J. Mech. Appl. Math., 53 (2000), pp. 565–582.
[16] F. T. Trouton, *On the coefficient of viscous traction and its relation to that of viscosity*, Proc. Roy. Soc. A, 77 (1906), pp. 426–440.
[17] D. Vaynblat, J. R. Lister, and T. P. Witelski, *Symmetry and self-similarity in rupture and pinchoff: A geometric bifurcation*, European J. Appl. Math., 12 (2001), pp. 209–232.
[18] E. D. Wilkes, S. D. Phillips, and O. A. Basaran, *Computational and experimental analysis of dynamics of drop formation*, Phys. Fluids, 11 (1999), pp. 3577–3598.
[19] S. D. R. Wilson, *The slow dripping of a viscous fluid*, J. Fluid Mech., 190 (1988), pp. 561–570.
[20] D. F. Zhang and H. A. Stone, *Drop formation in viscous flows at a vertical capillary tube*, Phys. Fluids, 9 (1997), pp. 2234–2242.